Acta Crystallographica Section B
Structural Science
ISSN 0108-7681

Electron diffraction and microscopy study of the structure and microstructure of the hexagonal perovskite $Ba_3Ti_2MnO_9$

Christian Maunders,[a]* Harold J. Whitfield,[b] David G. Hay[c] and Joanne Etheridge[b]

[a]Brockhouse Institute for Materials Research, McMaster University, Hamilton L8S 4L9, Canada, [b]Department of Materials Engineering, Building 69, Monash University, Victoria 3800, Australia, and [c]CSIRO Manufacturing and Infrastructure Technology, Private Bag 33, Clayton South MDC, Victoria 3169, Australia

Correspondence e-mail: maunder@mcmaster.ca

Received 22 November 2006
Accepted 2 March 2007

This paper reports a structural and microstructural investigation of the hexagonal perovskite $Ba_3Ti_2MnO_9$ using electron microscopy and diffraction. Convergent-beam electron diffraction (CBED) revealed the structure has the non-centrosymmetric space group $P6_3mc$ (186) at room temperature and at ~ 110 K. Compared with the centrosymmetric parent structure $BaTiO_3$, with space group $P6_3/mmc$, this represents a break in mirror symmetry normal to the c axis. This implies the Ti and Mn atoms are ordered on alternate octahedral sites along the $\langle 0001 \rangle$ direction in $Ba_3Ti_2MnO_9$. Using high-resolution electron microscopy (HREM), we observed occasional 6H/12R interfaces on (0001) planes, however, no antiphase boundaries were observed, as were seen in $Ba_3Ti_2RuO_9$. Using powder X-ray Rietveld refinement we have measured the lattice parameters from polycrystalline samples to be $a = 5.6880 \pm 0.0005$, $c = 13.9223 \pm 0.0015$ Å at room temperature.

1. Introduction

The electronic and structural parameters of the lower-temperature cubic-derived phases of the perovskite system have been extensively investigated (Jona & Shirane, 1962; Goodenough & Longo, 1970; Nomura, 1978). In particular, the manganite perovskites have been extensively investigated because of the interesting relationship between conductivity and magnetic ordering found in compounds such as $La_{1-x}Ca_xMnO_3$ ($x = 0.33$; Jin *et al.*, 1994).

The hexagonal phase of the perovskite $BaTiO_3$, see Fig. 1 (Megaw, 1946), is generally only stable at temperatures above the cubic to hexagonal phase transition at 1703 K (see Fig. 2). However, two methods have been developed that stabilize the hexagonal phase at room temperature.

The first method is to rapidly cool $BaTiO_3$ crystals in a reducing atmosphere from above the cubic to hexagonal transition temperature to room temperature. However, this method only produces metastable preparations of $BaTiO_3$ (Eibl *et al.*, 1989).

The second method, which produces perfect, very stable crystals, requires the partial substitution of Ti in $BaTiO_3$ with other transition metal (TM) elements. This was originally demonstrated for the stoichiometry $Ba_3Ti_2MO_9$ (M = V, Cr, Mn, Fe, Co, Ru, Rh, Ir or Pt; Dickson *et al.*, 1961), but more recently (Grey *et al.*, 1998; Langhammer *et al.*, 2000; Keith *et al.*, 2004) other M concentrations such as $Ba(Ti_{1-x}M_x)O_{3-\delta}$ with $0.05 \leq x \leq 0.50$ (M = Mg, Al, Cr, Mn, Fe, Co, Zn, Ga, Ni or In) have also been shown to be effective.

The mechanism by which the hexagonal phase is stabilized through TM element substitution is still a subject for active discussion. Ren *et al.* (1994) proposed that the small size of the

Mn^{4+} ion, relative to the Ti ion it substitutes, may promote the cubic to hexagonal phase transition, whilst Dickson *et al.* (1961) and Takeuchi *et al.* (1995) have suggested that bonding between the *d* orbitals of Ti and the TM enables face-sharing of the Ti and TM octahedra, which encourages the formation of the hexagonal structure. For small dopant concentrations, it has also been proposed that a Jahn–Teller distortion may drive the transition (Langhammer *et al.*, 2000). It is also noted that stabilization only occurs in these ternary oxides with Ba as the *A* atom in ABO_3 (Blasse, 1964).

The first step in understanding this stabilization process is to determine the structure of these compounds, which in many cases has only been partially determined. Blasse (1964) has pointed out that one of the outstanding questions is whether the TM element occupies the face-sharing or corner-sharing octahedral site. In other words, whether the same (Ti-Ti) or different (Ti-TM) cations are located in adjacent face-sharing octahedra. This can be a difficult question to answer because the difference in diffracted intensities between the two cases can be very small and/or long-range Ti/TM ordering can be difficult to achieve for certain TM elemental substitutions. However, the different TM site configurations correspond to different space groups, so this question can be answered through the determination of the space group, if the highly sensitive technique of convergent-beam electron diffraction is used.

Previously we determined that the space group of the related hexagonal perovskite, $Ba_3Ti_2RuO_9$, is $P6_3mc$ (186) and that the Ti and Ru atoms are located on alternate octahedral sites along the *c* axis (Maunders, Etheridge *et al.*, 2005). In that case TiO_6 and RuO_6 units meet at face-sharing octahedra. We also observed coherent $\{10\bar{1}0\}$ grain boundaries. From HREM images and CBED patterns, we inferred that the order of the Ru and Ti atoms was reversed from one side of the boundary to the other. However, it cannot be assumed that $Ba_3Ti_2MnO_9$ will necessarily have the same TM atom ordering as its Ru analogue, given the variety of oxidation states that Mn can adopt. In its 4+ oxidation state, it has a preference for octahedral site symmetry, whilst in 3+ it has a tendency towards Jahn–Teller distortions. Furthermore, the high-resolution electron energy-loss spectra of the two compounds reveal significant differences between the O–*K* edge spectra (Radtke *et al.*, 2005; Maunders, Whitfield *et al.*, 2005). More specifically, the energy-loss near-edge structure within these spectra, which probes the site- and symmetry-projected density of unoccupied states, is different. (An analysis of these differences is in progress.) For these reasons it is important to determine the space group of $Ba_3Ti_2MnO_9$ in order to determine the site occupied by Mn and if any Mn–Ti ordering is present. This is the primary purpose of the study reported here.

In the present work Ti atoms are partially substituted by Mn to give stoichiometric $Ba_3Ti_2MnO_9$. Dickson *et al.* (1961) has shown that, for this stoichiometry, Mn substitutes for Ti on half of its fourfold sites so there is one substitution cation per Ti_2O_9 coordination group in the unit cell.

Convergent-beam electron diffraction has been used here to determine the space group of $Ba_3Ti_2MnO_9$ and hence the Ti–Mn ordering within the unit cell. HREM has been used to examine the microstructure.

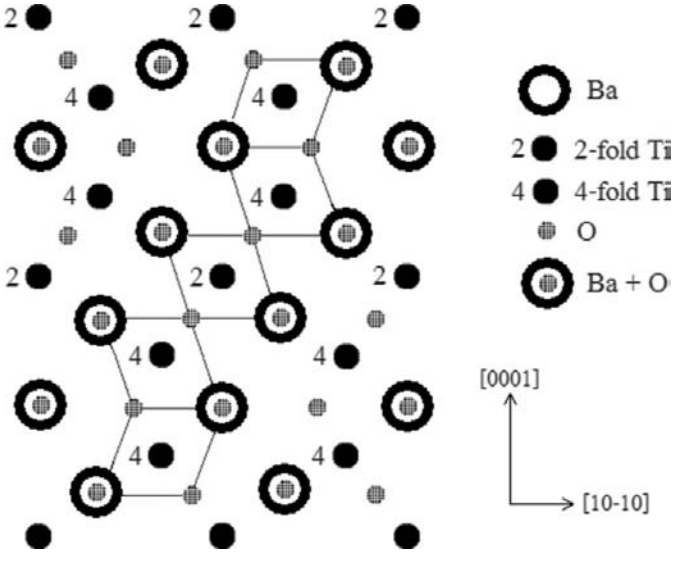

Figure 1
Hexagonal structure of $BaTiO_3$ projected along the $[2\bar{1}\bar{1}0]$ (from Maunders, Etheridge *et al.* 2005, reproduced with permission from the IUCr; http://journals.iucr.org), indicating two- and fourfold Ti sites and Ti_2O_9 coordination groups. The lattice parameters for the pure 6H hexagonal phase of $BaTiO_3$ were refined in a single-crystal X-ray study at 296 K as: a = 5.7238, c = 13.9649 Å (Akimoto *et al.*, 1994).

2. Experimental

A microcrystalline 2H polytype of $BaMn^{IV}O_3$ was prepared by heating barium manganate, $BaMn^{VI}O_4$, at 873 K for 24 h. Next, a weighed amount of titanium propoxide was diluted with ethanol and hydrolysed to a TiO_2 gel by the dropwise

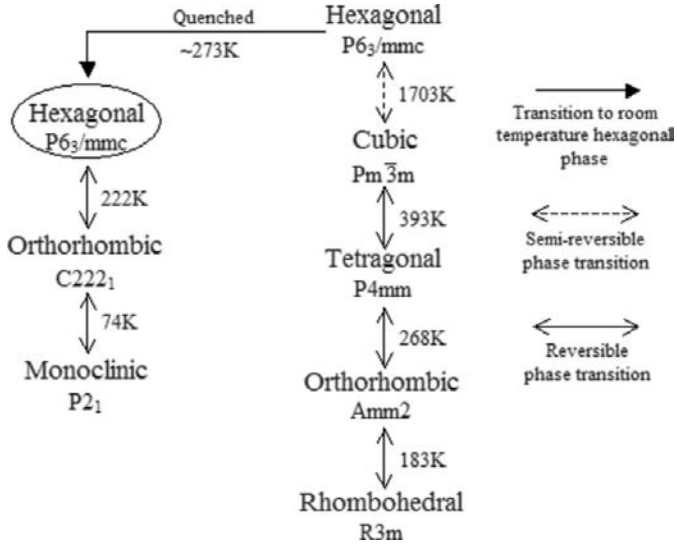

Figure 2
Transition temperatures and space-group symmetries of the phases of the $BaTiO_3$ perovskite system (from Maunders, Etheridge *et al.* 2005, reproduced with permission from the IUCr; http://journals.iucr.org).

addition of water. The titanium dioxide gel was dried and weighed amounts of barium carbonate and $BaMn^{IV}O_3$ were added to give a Ba:Ti:Mn stoichiometry ratio equal to 3:2:1. After grinding to a fine powder, the mixture was heated in an alumina crucible in a tube furnace in air to 1273 K for 48 h. The product was ground to a fine powder and reheated at 1273 K for a further 48 h to ensure complete reaction and formation of $Ba_3Ti_2MnO_9$.

Small single crystals were selected from the final preparation, crushed under ethanol and dispersed on a holey carbon Cu grid. This produced large, clean plate-like single crystals and avoided the surface damage and amorphization that occurs with other specimen preparation methods, particularly ion-beam thinning and polishing. It also provided a large array of such crystals per specimen grid, allowing many different crystals to be readily examined.

Crystals were found to be stable during selected-area electron diffraction (SAED), convergent-beam electron diffraction (CBED) and high-resolution electron microscope (HREM) imaging experiments which were performed in order to determine the stacking sequence, space group and microstructure. Energy-dispersive X-ray spectra were taken to confirm the stoichiometry.

The specimen was examined using a LaB_6 200 kV Jeol 2011 transmission electron microscope (TEM) fitted with an analytical pole piece and a FEG 200 kV Jeol 2010 TEM.

The lattice parameters of $Ba_3Ti_2MnO_9$ were measured with powder X-ray diffraction on a Bruker D8 X-ray diffractometer fitted with a graphite sample monochromator.

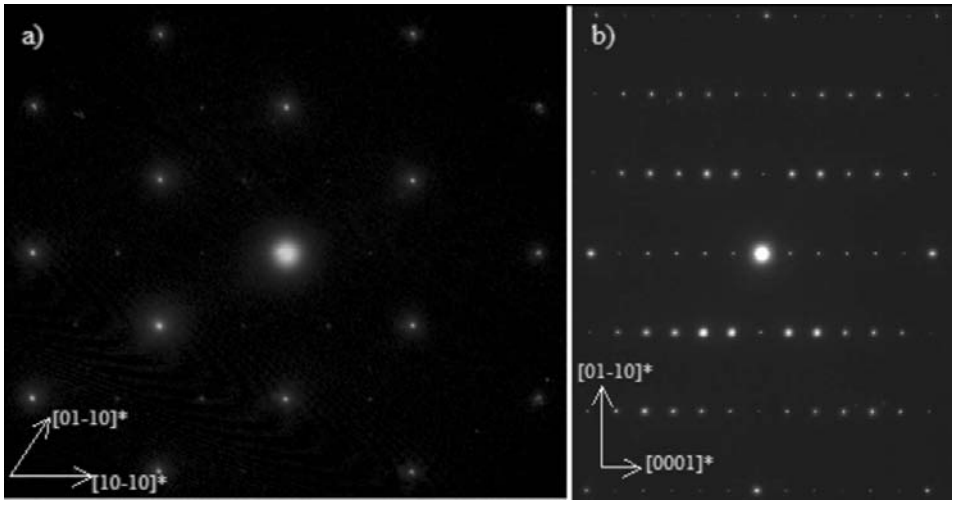

Figure 3
(*a*) [0001] and (*b*) $[2\bar{1}\bar{1}0]$ SAED patterns of $Ba_3Ti_2MnO_9$ consistent with a hexagonal unit cell with $(cch)_2$ stacking.

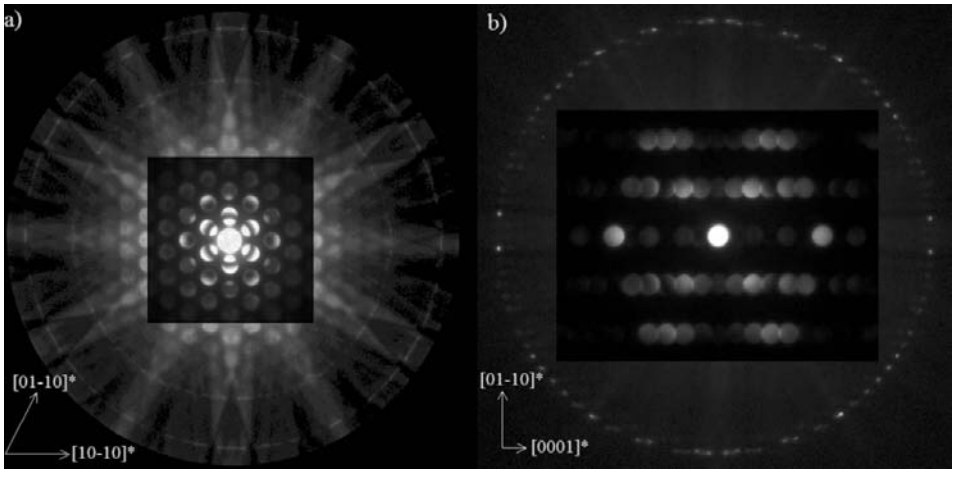

Figure 4
(*a*) [0001] CBED pattern of $Ba_3Ti_2MnO_9$ with 6*mm* symmetry. (*b*) $[2\bar{1}\bar{1}0]$ CBED pattern of $Ba_3Ti_2MnO_9$ with a mirror plane perpendicular to $[01\bar{1}0]$*, but no mirror plane perpendicular to [0001]* (compare, for example, the 0006 and $000\bar{6}$ reflections). The 2*mm* symmetry of the HOLZ confirm the beam is aligned precisely along the zone axis. (The HOLZ are displayed in *a* and *b* using a different intensity scale to the ZOLZ so that their 6*mm* and 2*mm* symmetries respectively are clear).

3. Results and discussion

3.1. Structure determination

Confirmation of the six-layer structure of hexagonal $BaTiO_3$, as proposed by Akimoto *et al.* (1994), was obtained from SAED patterns taken along the [0001] (Fig. 3*a*) and $[2\bar{1}\bar{1}0]$ (Fig. 3*b*) zone axes of $Ba_3Ti_2MnO_9$. These patterns are consistent with the $(cch)_2$ stacking sequence observed in $Ba_3Ti_2MnO_9$ by Dickson *et al.* (1961).

CBED can uniquely determine 218 of the 230 space groups (Goodman, 2001). In the following sections we use CBED to determine the space group of $Ba_3Ti_2MnO_9$ and consequently the Ti–Mn ordering on the fourfold sites parallel to the *c* axis. A unique determination of the space group of $Ba_3Ti_2MnO_9$ was achieved from CBED patterns taken along the [0001] and $[2\bar{1}\bar{1}0]$ zone axes and pairs of CBED patterns taken near the $[2\bar{1}\bar{1}0]$ zone axis.

3.1.1. Point group. The [0001] and $[2\bar{1}\bar{1}0]$ CBED patterns taken from $Ba_3Ti_2MnO_9$ are given in Figs. 4(*a*) and (*b*), respectively. The [0001] and $[2\bar{1}\bar{1}0]$ CBED patterns were taken at a nominal temperature of 110 K using a liquid nitrogen cooling holder. The specimen was cooled in order to reduce diffuse

Table 1
A comparison between the lattice parameters of $Ba_3Ti_2MnO_9$ and those of hexagonal $BaTiO_3$ determined by Akimoto *et al.* (1994).

	a (Å)	*c* (Å)	*c*/*a*
$Ba_3Ti_2MnO_9$	5.6880 ± 0.0005	13.9223 ± 0.0015	2.44766
Hexagonal $BaTiO_3$	5.7238 (7)	13.9649 (7)	2.43980

scattering and hence clarify the detail, particularly in the HOLZ discs. Room-temperature analogues of this pattern exhibited the same symmetry elements.

The [0001] CBED pattern shows 6*mm* whole pattern (WP) symmetry, consistent with the point groups 6*mm* or 6/*mmm* (Buxton *et al.*, 1976).

The $[2\bar{1}\bar{1}0]$ CBED pattern shows *m* WP symmetry. This is not a trivial observation made from a single pattern, but required careful analysis of many patterns. Fig. 4(*b*) is typical of all these patterns. They exhibit subtle differences in the intensity distribution between certain pairs of 000*l* and $000\bar{l}$ (*l* even) ZOLZ reflections, for example the $0006/000\bar{6}$ and $0002/000\bar{2}$ reflection pairs. The HOLZ reflections appear consistently to have 2*mm* symmetry (which also proved helpful in ensuring the precise alignment of the incident beam with the $[2\bar{1}\bar{1}0]$ zone axis). Whilst subtle differences in intensity can be generated by imperfect specimens, the nature of these differences will vary from specimen to specimen, depending on the nature of the imperfection. In particular, different pairs of reflections will be affected and different symmetry elements will be removed. This is *not* what we observed here. On the contrary, we consistently found in all of the patterns taken from many different specimens that the same mirror symmetry was absent and it was broken typically by the same pairs of reflections. We therefore deduced that the absence of this mirror symmetry is intrinsic to the crystal structure rather than an artefact generated by specimen geometry.

We note that CBED patterns recorded in the $[2\bar{1}\bar{1}0]$ zone axis from $Ba_3Ti_2RuO_9$ (Maunders, Etheridge *et al.*, 2005) also demonstrated a subtle break in mirror symmetry perpendicular to the *c* axis, as observed in $Ba_3Ti_2MnO_9$. As in the $Ba_3Ti_2RuO_9$ case, the mirror break persisted in the same pairs of ZOLZ reflections for a variety of crystal thicknesses. In the present case, the symmetry break might be expected to be particularly subtle, given it is generated by the substitution of Ti ($Z = 22$) with an element of close atomic number, Mn ($Z = 25$).

Given the subtlety of the above effect, we sought further evidence for the break in mirror symmetry perpendicular to the *c* axis using the method of Goodman (Goodman & Lehmpfuhl, 1968; Goodman, 1975, 2001) comparing conjugate reflection pairs, g and $\bar{g}$. The experiment was conducted specifically using reflection pairs in which the mirror break was observed in the zone-axis patterns.

In Fig. 5(*a*) a small tilt from the $[2\bar{1}\bar{1}0]$ zone axis sets the 0006 reflection close to the Bragg condition, whilst in Fig. 5(*b*) a tilt from the zone axis of equal magnitude but of opposite direction leaves the $000\bar{6}$ reflection close to the Bragg condition. The difference in intensity distribution in the 0006 and $000\bar{6}$ reflections (upper arrow) is obvious, whereas the $000\bar{6}$ and 0006 reflections of Figs. 5(*a*) and (*b*), respectively, have very similar intensity. This observation further demonstrates the break in mirror symmetry perpendicular to the *c* axis in the $[2\bar{1}\bar{1}0]$ zone-axis pattern.

Knowing only the WP symmetry *m* and not the bright field (BF) symmetry, the possible diffraction groups are *m*, $m1_R$ and 2_Rmm_R. The $g/\bar{g}$ experiment (Figs. 5*a* and *b*) demonstrated a symmetry of 1 between the 0006 and $000\bar{6}$ reflections and therefore the diffraction group 2_Rmm_R can be ruled out considering it has a $g/\bar{g}$ symmetry of 2_R.

The possible point groups resulting from the remaining *m* and $m1_R$ diffraction groups are *m*, *mm*2, 4*mm*, $\bar{4}2m$, 3*m*, $\bar{6}$, 6*mm*, $\bar{6}m2$, $\bar{4}3m$ and *mm*2, 4*mm*, $\bar{4}2m$, 6*mm*, $\bar{6}m2$, $\bar{4}3m$ (Buxton *et al.*, 1976). The only point group consistent with both the [0001] and $[2\bar{1}\bar{1}0]$ zone-axis pattern symmetries is 6*mm*. The break in mirror symmetry observed in the $[2\bar{1}\bar{1}0]$ zone-axis pattern is ultimately responsible for the distinction between the point groups 6*mm* and 6/*mmm*.

3.1.2. Space group. An important, but again subtle, feature of the $[2\bar{1}\bar{1}0]$ CBED pattern (Fig. 4*b*) are the Gjonnes–Moodie (G–M) extinction lines (Gjønnes &

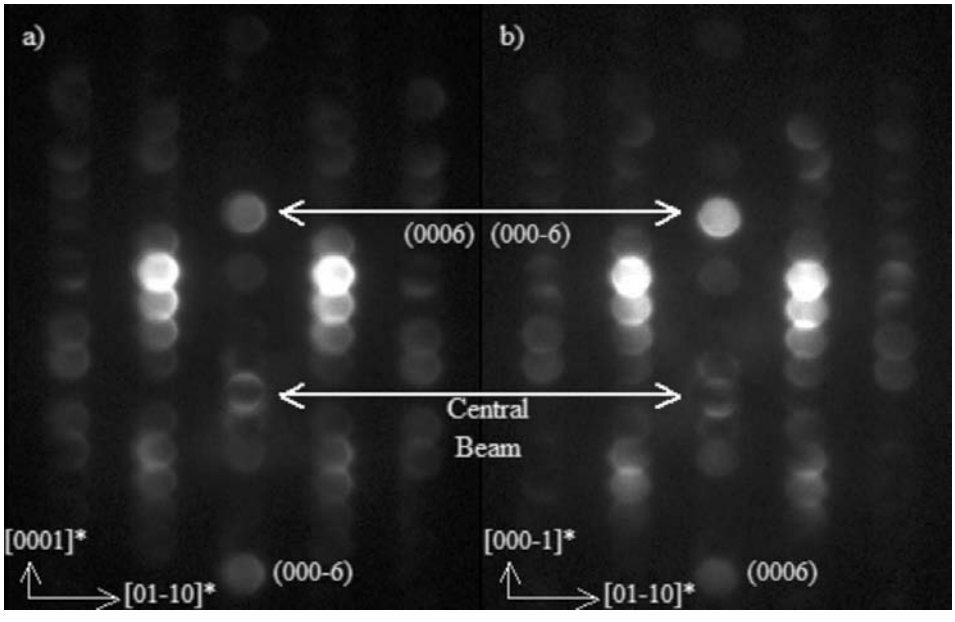

Figure 5
Comparison of conjugate pairs: CBED patterns of $Ba_3Ti_2MnO_9$ taken with (*a*) 0006 and (*b*) $000\bar{6}$ close to the Bragg angle.

Moodie, 1965; also observed in Figs. 5*a* and *b*) in the odd order (000*l*) reflections, which represent the translational symmetry element; the *c*-glide line. Considering this and the 6*mm* point-group symmetry the only possible space group is $P6_3mc$ (186); a reduction in symmetry from the space group $P6_3/mmc$ (194) of pure hexagonal $BaTiO_3$ (Burbank & Evans, 1948). The mirror break perpendicular to the *c* axis, as seen in Fig. 4(*b*), is at the origin of the loss in symmetry.

The combination of the break in mirror symmetry and the presence of the *c*-glide symmetry allows for the unique determination of the arrangement of the Mn and Ti atoms on the fourfold sites. To satisfy both of these symmetry conditions the Mn and Ti atoms must alternate on the fourfold sites (see Fig. 6). The Mn and Ti are consequently always in adjacent face-sharing octahedra (as proposed by Dickson *et al.*, 1961).

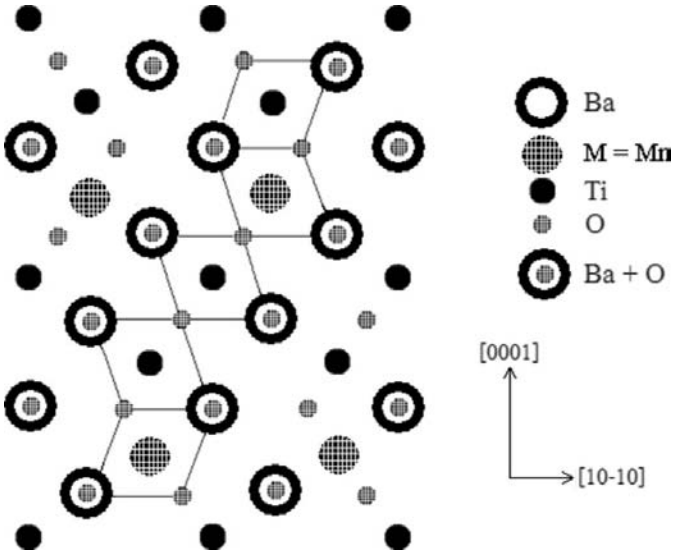

Figure 6
Scheme of the structure of $Ba_3Ti_2MnO_9$ in the $[2\bar{1}\bar{1}0]$ projection indicating the alternate Mn and Ti atom positions which are uniquely defined by the space-group symmetry.

3.2. Lattice parameter determination

The lattice parameters of $Ba_3Ti_2MnO_9$ were measured with powder X-ray diffraction on a Bruker D8 X-ray diffractometer fitted with a graphite sample monochromator. Cu $K\alpha$ radiation was used with a 2θ scan range of 2–92° at room temperature. A Rietveld refinement of the data collected, assuming the atomic model and space group determined above, gave the lattice parameters presented in Table 1.

Both the *a* and *c* axis of $Ba_3Ti_2MnO_9$ are shorter, within experimental error, than those of hexagonal $BaTiO_3$, as measured by Akimoto *et al.* (1994) from X-ray single-crystal measurements. The *c*/*a* ratio is consistent with the work of Zandbergen & Ijdo (1983, 1984), who reported a systematic increase in *c*/*a* for a series of $Ba_3MM'_2O_9$ perovskites as the difference in the atomic radii of *M* and *M*′ increases. They suggested that the reason for this is as follows. Since the *M* and *M*′ atoms have a different atomic radii, the size of their oxygen octahedral cages will also be different. The stacking of these different sized octahedra results in too much 'space' for the Ba atom and to reduce this space a tilt of the octahedra around their threefold axis occurs. Consequently, a slight decrease in the *a* axis length occurs, accompanied by an increase in *c*/*a*. However, if this occurs the tertiary *c* glides will be lost and the structure will no longer be consistent with the $P6_3mc$ space group. Hence we deduce this mechanism is *not* operative in $Ba_3Ti_2MnO_9$.

The decrease in the *c* axis of $Ba_3Ti_2MnO_9$, relative to hexagonal $BaTiO_3$, has also been observed in $BaTi_{1-x}Mn_xO_3$ for the small dopant concentrations $0.005 \leq x \leq 0.04$ (Kirianov *et al.*, 2001). In that work it was proposed that the *c*-axis contraction was due to the presence of Mn^{4+} or Mn^{3+} (with exchange energy lower than the crystal-field

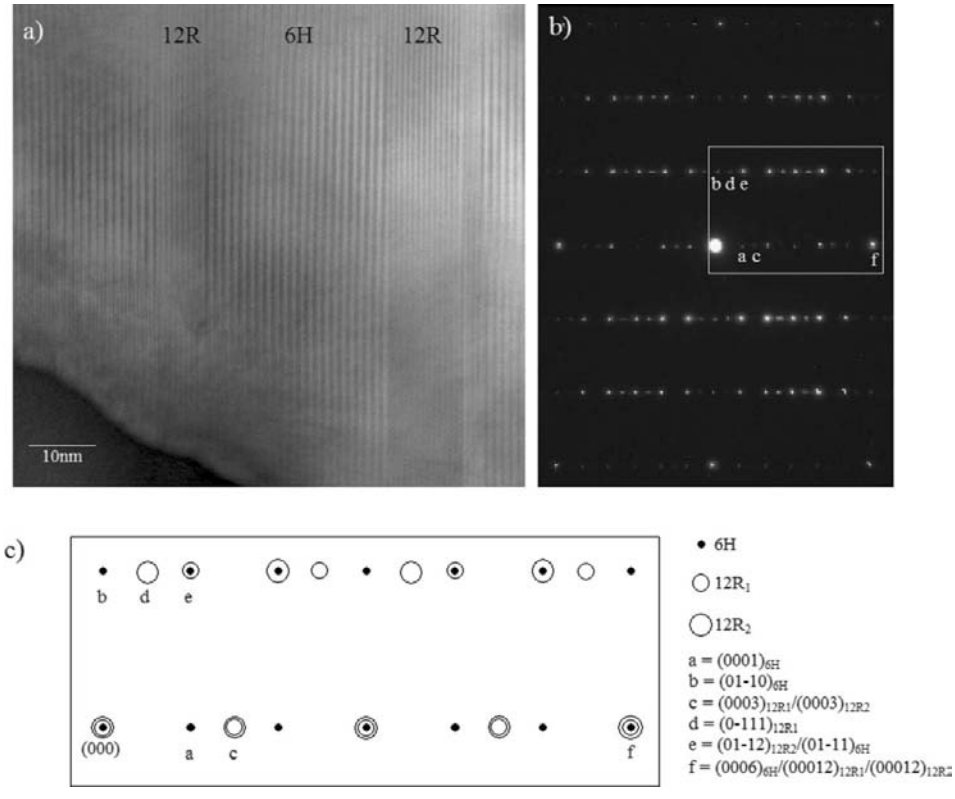

Figure 7
(*a*) HREM image of 6H/12R interfaces. (*b*) SAED pattern of the region shown in (*a*). (*c*) indexed diffraction pattern of boxed region in (*b*). Indexed reflections from the 6H and two 12R phases, 12R1 and 12R2 are given. 6H reflections are represented by closed small circles, 12R1 by small open circles and 12R2 by large open circles.

splitting), which have smaller ionic radii (0.530 and 0.580 Å; Shannon, 1976) than Ti^{4+} (0.605 Å). This might also be the case for $Ba_3Ti_2MnO_9$. The formal valency of Mn in $Ba_3Ti_2MnO_9$ was recently determined to be 4+ from ELNES studies (Radtke *et al.*, 2005), excluding the presence of Mn^{3+}.

3.3. Microstructure

HREM and SAED were used to examine the microstructure of $Ba_3Ti_2MnO_9$. Interfaces of 6H and 12R phases were occasionally observed on (0001) planes (see Fig. 7*a*). The SAED pattern of Fig. 7(*b*) is the result of the overlap of three independent structures in the field of view selected by the intermediate aperture, the 6H phase and two bands of a 12R phase with an antiparallel *c* axis.

The interfaces highlight the low energy difference between the 6H and the 12R structures. These interfaces were not observed in the Ru analogue of this structure, $Ba_3Ti_2RuO_9$ (Maunders, 2005).

On the other hand, 'anti-phase' boundaries have been observed in $Ba_3Ti_2RuO_9$ (Maunders, Etheridge *et al.*, 2005), but none were observed in this Mn analogue.

4. Conclusions

Using CBED we have shown that the space group of hexagonal $Ba_3Ti_2MnO_9$ is non-centrosymmetric $P6_3mc$ (186), analogous to the structure of $Ba_3Ti_2RuO_9$ (Maunders, Etheridge *et al.*, 2005; Maunders, 2005). This implies the Mn atoms are located on alternate fourfold Ti sites along the *c* axis, in adjacent face-sharing octahedra.

Using X-ray powder diffraction Rietveld refinement we have measured the lattice parameters to be $a = 5.6880 \pm 0.0005$ and $c = 13.9223 \pm 0.0015$ Å at room temperature. These results are consistent with the observations of others on doped hexagonal perovskites.

Occasional 6H/12R interfaces were observed on (0001) planes using HREM.

We acknowledge useful discussions with G. A. Botton, C. J. Rossouw and thank R. Withers for pointing out the loss of the tertiary *c* glides in the presence of octahedral rotation. This work was facilitated by the Australian Research Council infrastructure grant LE0238381, the Natural Sciences and Engineering Research Council of Canada (NSERC) and McMaster University.

References

Akimoto, J., Gotoh, Y. & Oosawa, Y. (1994). *Acta Cryst.* C**50**, 160–161.
Blasse, G. J. (1964). *Inorg. Nucl. Chem.* **27**, 993–1003.
Burbank, R. D. & Evans, H. T. (1948). *Acta Cryst.* **1**, 330–336.
Buxton, B. F., Eades, J. A., Steeds, J. W. & Rackham, G. M. (1976). *Philos. Trans. R. Soc. London*, **281**, 171–193.
Dickson, J. G., Katz, L. & Ward, R. (1961). *J. Am. Chem. Soc.* **83**, 3026–3029.
Eibl, O., Pongratz, P. & Skalicky, P. (1989). *Philos. Mag.* **60**, 601–612.
Gjønnes, J. & Moodie, A. F. (1965). *Acta Cryst.* **19**, 65–67.
Goodenough, J. B. & Longo, J. M. (1970). *Landolt–Bornstein*, New Series, Group III, Vol. 4a, ch. 3. New York: Springer.
Goodman, P. (1975). *Acta Cryst.* A**31**, 804–810.
Goodman, P. (2001). *International Tables for Crystallography*, edited by U. Shmueli, Vol. B, pp. 285–306. Dordrecht: Kluwer Academic Publishers.
Goodman, P. & Lehmpfuhl, G. (1968). *Acta Cryst.* A**24**, 339–347.
Grey, I. E., Cranswick, L. M. D. & Li, C. (1998). *J. Appl. Cryst.* **31**, 692–699.
Jin, S., Tiefel, T. H., McCormack, M., Fastnacht, R. A., Ramesh, R. & Chen, L. H. (1994). *Science*, **264**, 413–415.
Jona, F. & Shirane, G. (1962). *Ferroelectric Crystals.* Oxford: Pergamon Press.
Keith, G. M., Rampling, M. J., Sarma, K., McAlford, N. & Sinclair, D. C. (2004). *J. Eur. Ceram. Soc.* **24**, 1721–1724.
Kirianov, A., Ozaki, N., Ohsato, H., Kouzu, N. & Kishi, H. (2001). *Jpn. J. Appl. Phys.* **40**, 5619–5623.
Langhammer, H. T., Muller, T., Felgner, K.-H. & Abicht, H.-P. (2000). *J. Am. Ceram. Soc.* **83**, 605–611.
Maunders, C. (2005). PhD Thesis, pp. 94. Materials Engineering, Monash University, Melbourne.
Maunders, C., Etheridge, J., Wright, N. & Whitfield, H. J. (2005). *Acta Cryst.* B**61**, 154–159.
Maunders, C., Whitfield, H. J., Radtke, G., Botton, G. A., Lazar, S. & Etheridge, J. (2005). *Proc. Microsc. Microanal.* **11** (suppl 2), 738.
Megaw, H. D. (1946). *Proc. Phys. Soc.* **58**, 133–152.
Nomura, S. (1978). *Landolt–Bornstein*, New Series, Group III, Vol. 12a, ch. 2. New York: Springer.
Radtke, G., Maunders, C., Lazar, S., De Groot, F. M. F., Etheridge, J. & Botton, G. A. (2005). *J. Solid State Chem.* **178**, 3426–3430.
Ren, F., Ishida, S. & Mineta, S. (1994). *J. Ceram. Soc. Jpn*, **102**, 106–108.
Shannon, R. D. (1976). *Acta Cryst.* A**32**, 751–767.
Takeuchi, N., Ishida, S. & Wakamatsu, M. (1995). *Memoirs of the Faculty of Engineering and Design*, Vol. 43, pp. 51–66. Kyoto Institute of Technology, Japan.
Zandbergen, H. W. & Ijdo, D. J. W. (1983). *Acta Cryst.* C**39**, 829–832.
Zandbergen, H. W. & Ijdo, D. J. W. (1984). *Acta Cryst.* C**40**, 919–922.